Journal of Pathology
J Pathol (2012)
Published online in Wiley Online Library
(wileyonlinelibrary.com) DOI: 10.1002/path.4043

ORIGINAL PAPER

Cellular ageing, increased mortality and FTLD-TDP-associated neuropathology in progranulin knockout mice

Hans Wils,[1,2†] Gernot Kleinberger,[1,2†] Sandra Pereson,[1,2] Jonathan Janssens,[1,2] Anja Capell,[3] Debby Van Dam,[4] Ivy Cuijt,[1,2] Geert Joris,[1,2] Peter P De Deyn,[4] Christian Haass,[3,5] Christine Van Broeckhoven[1,2*] and Samir Kumar-Singh[1,2*]

[1] *Neurodegenerative Brain Diseases Group, Department of Molecular Genetics, VIB, Antwerp, Belgium*
[2] *Laboratory of Neurogenetics, Institute Born-Bunge, University of Antwerp, Antwerp, Belgium*
[3] *Adolf-Butenandt-Institute, Biochemistry, Ludwig-Maximilians-University Munich, Munich, Germany*
[4] *Laboratory of Neurochemistry and Behavior, Institute Born-Bunge, University of Antwerp, Antwerp, Belgium*
[5] *German Center for Neurodegenerative Diseases (DZNE), Munich, Munich, Germany*

**Correspondence to: Professor Dr Christine Van Broeckhoven, PhD, DSc, Neurodegenerative Brain Diseases Group, VIB Department of Molecular Genetics, University of Antwerp—CDE, Universiteitsplein 1, B-2610, Antwerp, Belgium. e-mail: christine.vanbroeckhoven@molgen.vib-ua.be or Professor Dr Samir Kumar-Singh, MD, PhD. Current address: Molecular and Cellular Neuropathology Group, Laboratory of Cell Biology and Histology, University of Antwerp–CDE, Universiteitsplein 1, B-2610, Antwerp, Belgium. e-mail: samir.kumarsingh@ua.ac.be*

†These authors contributed equally to this work.

Abstract

Loss-of-function mutations in *progranulin* (*GRN*) are associated with frontotemporal lobar degeneration with intraneuronal ubiquitinated protein accumulations composed primarily of hyperphosphorylated TDP-43 (FTLD-TDP). The mechanism by which GRN deficiency causes TDP-43 pathology or neurodegeneration remains elusive. To explore the role of GRN *in vivo*, we established *Grn* knockout mice using a targeted genomic recombination approach and *Cre-LoxP* technology. Constitutive *Grn* homozygous knockout ($Grn^{-/-}$) mice were born in an expected Mendelian pattern of inheritance and showed no phenotypic alterations compared to heterozygous ($Grn^{+/-}$) or wild-type (Wt) littermates until 10 months of age. From then, $Grn^{-/-}$ mice showed reduced survival accompanied by significantly increased gliosis and ubiquitin-positive accumulations in the cortex, hippocampus, and subcortical regions. Although phosphorylated TDP-43 could not be detected in the ubiquitinated inclusions, elevated levels of hyperphosphorylated full-length TDP-43 were recovered from detergent-insoluble brain fractions of $Grn^{-/-}$ mice. Phosphorylated TDP-43 increased with age and was primarily extracted from the nuclear fraction. $Grn^{-/-}$ mice also showed degenerative liver changes and cathepsin D-positive foamy histiocytes within sinusoids, suggesting widespread defects in lysosomal turnover. An increase in insulin-like growth factor (IGF)-1 was observed in $Grn^{-/-}$ brains, and increased IGF-1 signalling has been associated with decreased longevity. Our data suggest that progranulin deficiency in mice leads to reduced survival in adulthood and increased cellular ageing accompanied by hyperphosphorylation of TDP-43, and recapitulates key aspects of FTLD-TDP neuropathology.

Keywords: progranulin; TDP-43; FTLD; ageing; liver pathology; mouse model; IGF-1

Received 24 October 2011; Revised 31 March 2012; Accepted 14 April 2012

No conflicts of interest were declared.

Introduction

Recently, loss-of-function mutations in *progranulin* (*GRN*) have been identified as an important cause of frontotemporal lobar degeneration with ubiquitin-positive, tau-negative inclusions (FTLD-U) [1,2]. GRN is a secreted precursor glycoprotein that is proteolytically cleaved to form granulin peptides, and both GRN and granulin peptides serve as multifunctional growth factors with important roles in development, cell cycle progression, cell motility, wound repair, neurite outgrowth, and inflammation [3,4]. The precise function of GRN in the brain and the mechanism by which GRN haploinsufficiency leads to neurodegeneration are currently unknown [5]. GRN binds to sortilin, leading to rapid endocytosis and lysosomal localization of the sortilin–GRN complex, thus controlling the levels of GRN [6]. GRN also binds directly to tumour necrosis factor receptors (TNFRs) and acts as an antagonist of TNFα signalling [7].

TAR DNA-binding protein 43 (TDP-43), a member of the heterogeneous ribonucleoprotein (hnRNP) family involved in regulation of transcription and splicing, is a major protein constituent of the ubiquitinated inclusions in the majority of FTLD-U (or FTLD-TDP) [8–10]. In affected brain regions, TDP-43

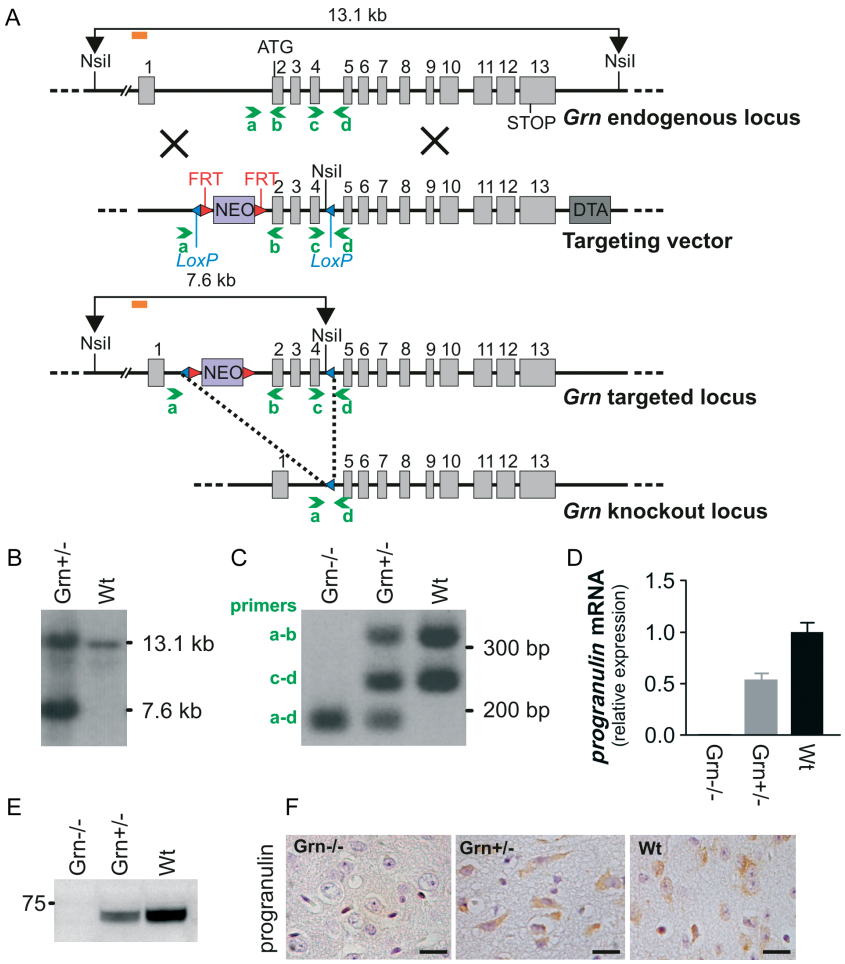

Figure 1. Generation of constitutive *Grn* knockout ($Grn^{-/-}$) mice. (A) Schematic drawing of the targeting strategy for the *Grn* locus. Light grey boxes represent exons. Neomycin resistance gene (NEO; purple), diphtheria toxin A (DTA; dark grey), *LoxP* sites (blue triangles), and FRT recombination target sites (red triangles) are indicated. (B) Southern blot of *NsiI*-digested heterozygous $Grn^{+/-}$ and wild-type (Wt) genomic DNA hybridized with a 5′ probe located external from the targeting vector (probe is depicted as an orange rectangle in A). (C) PCR analysis from tail biopsies showing a band of 195 bp for homozygous $Grn^{-/-}$ mice and a band of 258 bp and 344 bp for Wt mice (primers are depicted as green arrows labelled a–d in A). (D) qRT-PCR on total brain lysates with primers spanning the exon 3–4 junction showing total progranulin mRNA expression relative to Wt. Data are represented as mean ± SD. (E) Immunoblotting for mouse Grn showing reduced full-length protein expression in $Grn^{+/-}$ mice, which is absent in $Grn^{-/-}$ mice. (F) Progranulin immunohistochemistry showing absence of staining in $Grn^{-/-}$ mice but its presence in $Grn^{+/-}$ and Wt littermates. Scale bars = 20 µm.

is abnormally ubiquitinated, phosphorylated, and C-terminal 25–35 kDa fragments accumulate [8,9,11]. Here, we report that allelic deficiency of *Grn* in mice leads to disease characteristic features of FTLD-TDP such as phosphorylation of TDP-43, increased signs of cellular ageing of neuronal and non-neuronal tissue, and decreased lifespan.

Materials and methods

Generation of *Grn* knockout ($Grn^{-/-}$) mice

$Grn^{-/-}$ mice were generated by cloning ≈ 11.7 kb fragment including *Grn* from a mouse 129/Sv BAC clone (#bMQ-242E3; Sanger Institute, Cambridge, UK) into a pZeroTM-1 vector (Life Technologies, Merelbeke, Belgium). Using targeted genomic mutagenesis, two *LoxP* sites were inserted flanking *Grn* exons 2 and 4 for eventual deletion of the Start-ATG, signal peptide, and first Grn peptide (Figure 1A). A neomycin resistance gene flanked with FRT sites and a diphtheria toxin (DTA) cassette were used for positive and negative selection, respectively. Homologous recombination was validated by Southern blotting (Figure 1B). The targeting construct was linearized and electroporated into 129/Sv embryonic stem (ES) cells (GenOway, Lyon, France). Recombinant ES cells were expanded and two independent ES cell lines were injected into C57BL/6J blastocysts and transferred into pseudo-pregnant females. Five pups were born, of which three males displayed a chimerism rate of 80%. These were bred with mice ubiquitously expressing *Cre*-recombinase to generate heterozygous $Grn^{+/-}$ mice. $Grn^{+/-}$ mice were inter-crossed to generate homozygous $Grn^{-/-}$ mice on a mixed Bl6/129Sv background. All animal experiments were approved by the University of Antwerp Ethics Committee and conducted according to the guidelines of the Federation of European Laboratory Animal Science Associations.

Behavioural studies

Behavioural analysis was performed on Grn$^{-/-}$ and Wt mice of 13–15 ($n = 10$ and 12 males) and 20–22 months of age ($n = 8$ females per group) as described in the Supporting information, Supplementary methods.

Immunoblotting, immunohistochemistry (IHC), and quantitative real-time PCR (qRT-PCR)

Cytoplasmic and nuclear brain extracts as well as brain lysates extracted with detergents of increasing ionic strength were prepared as described previously [12–14]. Classical histochemistry and IHC were performed according to standard protocols [15], utilizing the antibodies enumerated in the Supporting information, Supplementary Table 1. Preparation of tissue, and quantitative and semi-quantitative immunohistochemical analyses were performed as described earlier [15]. qRT-PCR analysis was performed on total brain RNA using SYBR Green technology with primers listed in the Supporting information, Supplementary Table 2.

Results

Generation and molecular characterization of *Grn* knockout (Grn$^{-/-}$) mice

To study the role of GRN loss-of-function in FTLD-TDP pathology, we established *Grn* knockout (Grn$^{-/-}$) mice (Figure 1). Recombination and zygosity were validated by Southern blotting and PCR (Figures 1B and 1C). qRT-PCR showed ≈ 50% reduced expression of total *Grn* transcript in the brains of Grn$^{+/-}$ mice, which was not detectable in Grn$^{-/-}$ mice (Figure 1D). Loss of full-length Grn was confirmed by mouse Grn immunoblotting (Figure 1E). Although we cannot exclude the potential expression of individual granulin peptides or an N-truncated Grn protein originating from an alternative ATG, these would be produced in very low quantities (Supporting information, Supplementary Figure 1). Anti-Grn IHC showed no detectable reactivity in Grn$^{-/-}$ mice, while an expected Grn expression pattern was observed in neuronal and glial cells in Wt and Grn$^{+/-}$ mice (Figure 1F).

Decreased survival in aged Grn$^{-/-}$ mice

Crossbreeding of Grn$^{+/-}$ mice generated 24.3% Grn$^{-/-}$, 45.0% Grn$^{+/-}$, and 30.7% Wt mice, a pattern approaching Mendelian distribution without decreased frequency in Grn$^{-/-}$ mice (expected, 25%, 50%, and 25%). Young adult Grn$^{-/-}$ mice were fertile and appeared healthy until 10 months of age, when they started to show increased mortality compared with Grn$^{+/-}$ and Wt mice (Figure 2A; $p < 0.001$). The relative risk of dying increased exponentially with age, with Grn$^{-/-}$ mice showing a 17.5-fold higher probability of dying at 23.5 months compared with

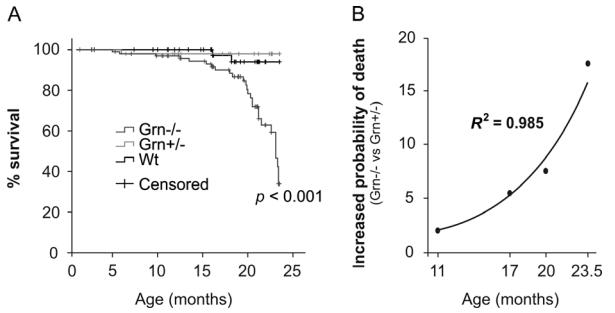

Figure 2. Decreased survival in aged Grn$^{-/-}$ mice. (A) Increased mortality is observed after 10 months of age in Grn$^{-/-}$ mice compared with Grn$^{+/-}$ and Wt mice. (B) Probability of death for Grn$^{-/-}$ mice increased exponentially with age compared with Grn$^{+/-}$ littermates. Mantel–Cox survival analysis, $p < 0.001$, $\chi^2 = 15.9$, df = 2.

Grn$^{+/-}$ littermates (Figure 2B). Routine ELISA-based tests showed absence of important mouse pathogens (including hepatitis, parvo, encephalomyelitis, reo, rota, sendai, and minute virus, and *Mycoplasma pulmonis*) responsible for early mortality in animal facilities.

To study whether Grn$^{-/-}$ mice present cognitive or behavioural deficits at the onset of increased mortality, or at later time-points when mortality increases drastically, Grn$^{-/-}$ and Wt mice of 13–15 and 20–22 months were subjected to several assays. No significant deficits in exploration and anxiety, circadian locomotor activity, motor performance or contextual learning were observed. Only by Morris water maze was a reduced efficiency of Grn$^{-/-}$ mice in finding the invisible platform during acquisition trials detected (Supporting information, Supplementary Figure 2).

Increased gliosis in aged Grn$^{-/-}$ mice

Because progranulin and granulin peptides are involved in inflammation, we questioned whether Grn$^{-/-}$ mice displayed any obvious changes in gliosis. Anti-GFAP IHC performed on ≈ 6-, ≈ 12-, and ≈ 21-month-old Grn$^{-/-}$ mice showed astrogliosis in deeper cortical layers, hippocampus, and several subcortical regions that increased with age compared with Wt littermates (Figure 3A and Supporting information, Supplementary Figure 3A; $p < 0.001$). Similarly, Iba1 and ferritin staining for (activated) microglia detected increased microgliosis in Grn$^{-/-}$ mice for all analysed ages (Figure 3B and Supporting information, Supplementary Figure 3B; $p < 0.01$), especially in subcortical regions and to a lesser degree in the hippocampus. Consistent with a recently reported Grn$^{-/-}$ mouse model [16], heterozygous Grn$^{+/-}$ mice were indistinguishable from Wt littermates.

Accumulation of ubiquitinated proteins and impaired autophagy–lysosomal pathway in aged Grn$^{-/-}$ brain

Grn$^{-/-}$ mice showed progressive brain ubiquitin pathology as diffuse and granular cytoplasmic neuronal staining in the cortex, CA hippocampus, subiculum,

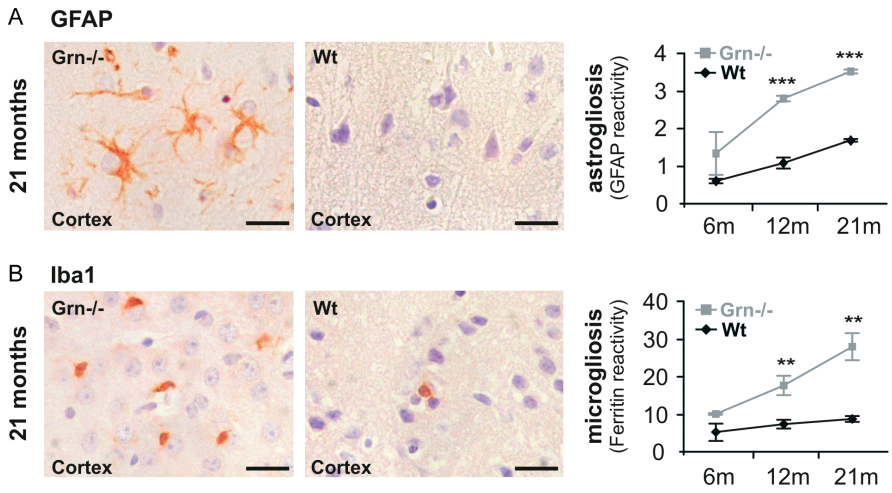

Figure 3. Increased gliosis in aged $Grn^{-/-}$ mice. (A) Increased astrogliosis (GFAP) and (B) elevated microglial activation (Iba1) in the deeper layers of the cortex in $Grn^{-/-}$ mice compared with Wt littermates. Right panel shows quantification of astrogliosis and microgliosis (by ferritin staining) observed in the brains of 6-, 12-, and 21-month-old $Grn^{-/-}$ and Wt mice ($n \geq 3$ mice for each group). Scale bars = 20 µm. Data are represented as mean ± SD. $^{**}p < 0.01$; $^{***}p < 0.001$.

dentate gyrus, thalamus, and other subcortical regions (Figure 4A and Supporting information, Supplementary Figure 4A). Large, well-defined, circumscribed, cytoplasmic cellular accumulations of up to 4 µm in diameter were also observed in these regions. Ubiquitin neuritic pathology was remarkable in $Grn^{-/-}$ mice, especially in the subcortical regions. Wt littermates also showed ubiquitin immunostaining as diffuse, granular, or small cytoplasmic cellular accumulations, especially in the CA2–3 hippocampus. Quantification of neurons with ubiquitin immunoreactivity showed a significant 2.3-, 1.7-, and 2-fold increase in ≈ 6-, ≈ 12-, and ≈ 21-month-old $Grn^{-/-}$ mice compared with Wt littermates (Figure 4A, right panel; $p < 0.01$ for all ages). Furthermore, a significant 6.5-, 1.5-, and 9-fold increase in ubiquitin immunoreactivity was observed in the cortex, hippocampus, and thalamus, respectively, in ≈ 21-month-old $Grn^{-/-}$ mice compared with Wt littermates (Supporting information, Supplementary Figure 4B). Consistent with the IHC data, immunoblotting with an anti-Ub antibody showed increased levels of polyubiquitinated proteins in the brains of $Grn^{-/-}$ mice (Supporting information, Supplementary Figure 4C), suggesting disturbance in the ubiquitin–proteasome system, a characteristic feature of FTLD-TDP [17].

In addition, $Grn^{-/-}$ mice also showed an age-dependent 2-fold increase in autofluorescent lipofuscin pigment accumulation in many brain regions including the cortex, thalamus, and CA hippocampus (Figure 4B and Supporting information, Supplementary Figures 4D–4F). Abnormal accumulation of lipofuscin granules is characteristic of many neurodegenerative disorders and suggests impairment of the autophagy–lysosomal system [18]. Consistent with this premise, we observed in ≈ 18-month-old $Grn^{-/-}$ mice a significant 15-fold increased amount of cytosolic inclusions immunoreactive for autophagy receptor protein p62 (Figure 4C and Supporting information, Supplementary Figures 4G–4I), a protein known to accumulate in autophagy-deficient conditions [19]. p62 accumulation was confirmed by immunoblotting of RIPA insoluble urea fractions from $Grn^{-/-}$ mice (Supporting information, Supplementary Figure 4I). Furthermore, very intense immunoreactivity of lysosomal protease cathepsin D was also observed in specific brain areas of ≈ 18-month-old $Grn^{-/-}$ mice compared with age-matched controls (Figure 4D). qRT-PCR analysis on total brain extracts showed a highly significant 3-fold increase in cathepsin D (*Ctsd*; Figure 4E, $p < 0.01$), but also in cathepsins S and B (*Ctss* and *Ctsb)* (Supporting information, Supplementary Figures 4J and 4K). These data all suggest that $Grn^{-/-}$ mice not only have disturbances of the ubiquitin–proteasome system-mediated protein degradation, but also have disturbance of the autophagy–lysosomal system with alterations in lysosomal homeostasis, both being characteristic features of FTLD-TDP [20].

Increased phosphorylation of TDP-43 in aged $Grn^{-/-}$ mice

Full-length (FL) TDP-43 and its C-terminal fragments (CTFs) are identified as major protein constituents of the ubiquitinated inclusions observed in FTLD-TDP patients [8,9,21]. Utilizing TDP-43 antibodies against the C-terminus or holoprotein, no mislocalization of TDP-43 from its predominant nuclear location to the cytoplasm or presence in cytoplasmic ubiquitin inclusions was detected in $Grn^{-/-}$ mice. The ubiquitin inclusions were also not immunoreactive to tau, α-synuclein or FUS (Supporting information, Supplementary Figure 5). Weak nuclear immunoreactivity for phospho-TDP-43 (pTDP 409/410) was observed in both $Grn^{-/-}$ and Wt littermates without detectable alterations in $Grn^{-/-}$ mice. Interestingly, occasional neurons showed intense nuclear pTDP-43 staining, especially in $Grn^{-/-}$ mice (Figure 5A). These findings were further confirmed with another TDP-43

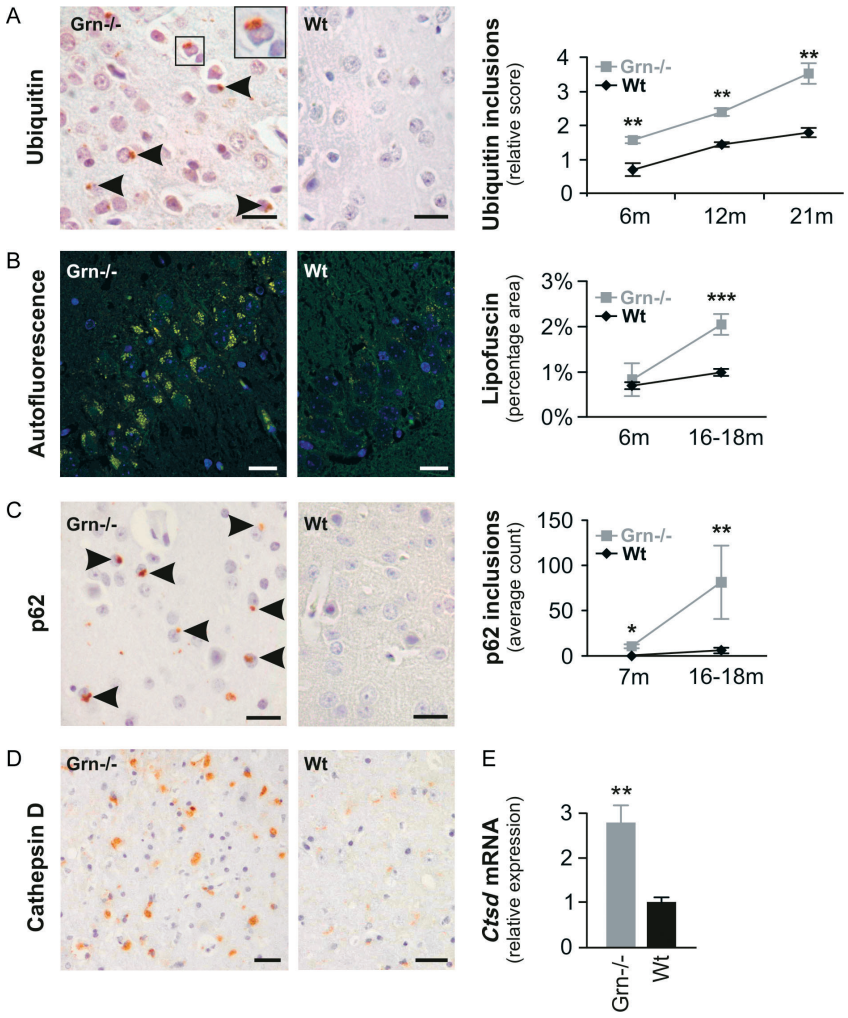

Figure 4. Disturbed ubiquitin–proteasome and autophagy–lysosomal degradation of proteins in aged Grn$^{-/-}$ mice. (A) Ubiquitin immunohistochemistry showing accumulations in the cortex of aged Grn$^{-/-}$ mice that are not present in Wt littermates. Inclusions are indicated by arrowheads and right panel shows quantification of ubiquitin reactivity in the brains of 6-, 12-, and 21-month-old Grn$^{-/-}$ and Wt mice ($n \geq 3$ mice for each group). (B) Increased autofluorescence in the hippocampus of Grn$^{-/-}$ mice compared with Wt littermates which was significantly increased in 16- to 18-month-old Grn$^{-/-}$ mice (average lipofuscin area of three different brain regions). (C) Frequently observed p62-positive inclusions in Grn$^{-/-}$ mice that are markedly larger and more abundant than in Wt mice. Inclusions are indicated by arrowheads and right panel shows quantification of p62 reactivity in the cortex and thalamus. Scale bars in A–D = 20 µm. (D) Increased cathepsin D immunoreactivity was observed in the thalamus, the area with the highest load of ubiquitin and p-62 accumulations, in aged Grn$^{-/-}$ mice. Right panel shows quantification of cathepsin D reactivity in the thalamus. (E) qRT-PCR analysis confirms significantly increased levels of the lysosomal protease cathepsin D (*Ctsd*). Data are represented as mean ± SD. $^{*}p < 0.05$; $^{**}p < 0.01$; $^{***}p < 0.001$.

phospho-specific antibody (pTDP 403/404) showing faint nuclear, but also cytoplasmic reactivity in cortical neurons more commonly in Grn$^{-/-}$ mice than in their Wt littermates (Supporting information, Supplementary Figure 6A). To study whether some of the intense staining could represent non-specific reactivity in apoptotic neurons, we analysed cleaved caspase-3 and TUNEL reactivity by IHC but did not identify significant differences between ≈ 18-month-old Grn$^{-/-}$ and Wt littermates (Supporting information, Supplementary Figures 7A and 7B). Furthermore, no significant differences were detected by immunoblotting for cleaved caspase-3 and cleaved PARP (Supporting information, Supplementary Figure 7C), suggesting that loss of Grn does not directly lead to apoptosis in our Grn$^{-/-}$ mouse model.

We further studied TDP-43 fragmentation in the brains of 21-month-old Grn$^{-/-}$ mice. Utilizing a pan-TDP-43 antibody, FL-TDP-43 was the major species identified in both Grn$^{-/-}$ and Wt mice. TDP-43 was RIPA-soluble, although a small proportion was also recovered in urea fractions and no TDP-43 CTFs were observed in the urea fraction (Figure 5B). After reprobing with pTDP 409/410 antibody, significantly increased levels of FL-pTDP-43 were detected in Grn$^{-/-}$ mice compared with Wt littermates (Figure 5C). These data were confirmed by pTDP-403/404 immunoblotting (Supporting information, Supplementary Figure 6B). Furthermore, an age-dependent accumulation of FL-pTDP-43 was observed in Grn$^{-/-}$ mice starting at the age of 12 months, with significantly increased pTDP-43 levels at 21 months of

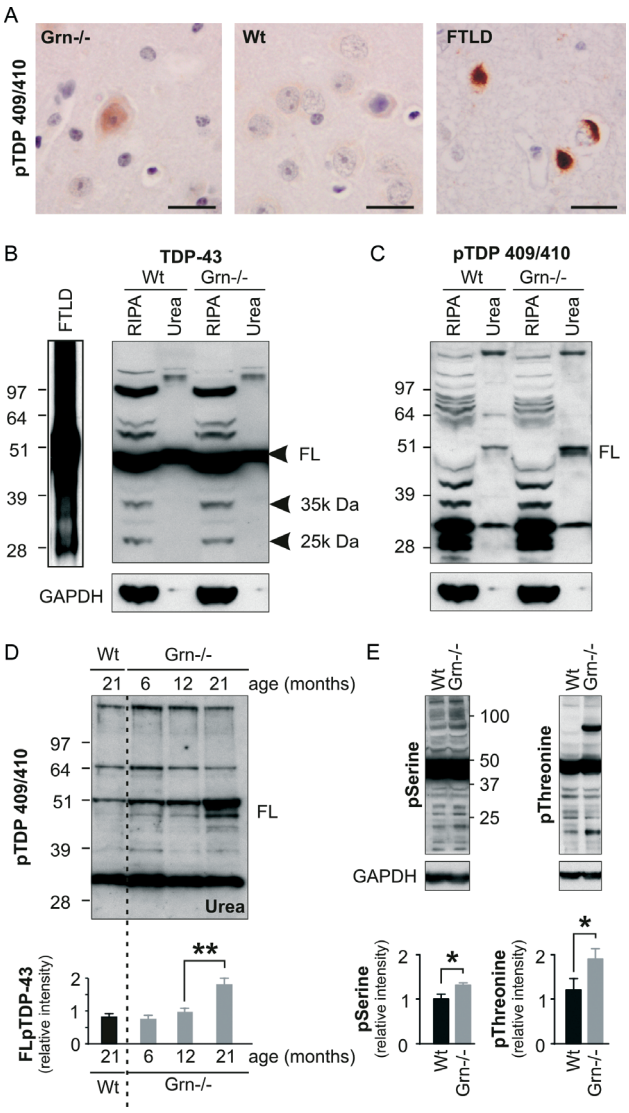

Figure 5. Increased phosphorylation of full-length (FL) TDP-43 in aged Grn$^{-/-}$ mice. (A) TDP-43 immunohistochemistry with polyclonal anti-phospho 409/410 TDP-43 (pTDP 409/410) showing occasional cellular staining that was, however, not significantly different between Grn$^{-/-}$ and Wt mice. An FTLD patient is shown for comparison. Bar = 20 µm. (B) Immunoblotting with a pan-TDP-43 antibody also did not show any apparent differences in the TDP-43 fragmentation pattern in Grn$^{-/-}$ mice compared with Wt littermates. A urea sample of a human FTLD patient was added as a reference. (C) Reprobing the same blot with the pTDP 409/410 antibody, however, detected bands at the height of FL phosphorylated TDP-43 in Grn$^{-/-}$ mice that were weak to absent in Wt mice. (D) Quantitative immunoblot analysis of the FL-pTDP-43 band with pTDP 409/410 antibody in 6-, 12-, and 21-month-old Grn$^{-/-}$ mice and 21-month-old Wt mice showing a significant increase in aged Grn$^{-/-}$ mice. (E) Quantitative immunoblot analysis with phosphoserine- or phosphothreonine-specific antibodies showed significantly increased total reactivity in Grn$^{-/-}$ mice compared with Wt mice for both antibodies. Data are represented as mean ± SD. $^{*}p < 0.05$; $^{**}p < 0.01$.

age (Figure 5D and Supporting information, Supplementary Figure 6C; $p < 0.01$). In contrast, Wt littermates showed only absent to weak FL-pTDP-43 until 24 months of age (Supporting information, Supplementary Figure 6D). Moreover, FL-pTDP-43 was primarily recovered from the nuclear, sarkosyl-soluble fraction from the brains of Grn$^{-/-}$ mice (Supporting information, Supplementary Figures 8A and 8B). Because progranulin is thought to be involved in important cell signalling pathways, we questioned whether increased phosphorylation of TDP-43 might simply represent a generally increased phosphorylation state of cellular proteins in Grn$^{-/-}$ cells. Utilizing antibodies against phosphoserines and phosphothreonines, we observed a small but significant increase in total phosphorylation states in the brains of Grn$^{-/-}$ mice (Figure 5E). These data all suggest that although loss of Grn does not substantially cause fragmentation or aggregation of TDP-43 in the ubiquitinated inclusions observed in our Grn$^{-/-}$ mice, loss of Grn does lead to increased phosphorylation states of proteins including FL-TDP-43.

Increased cellular ageing and liver pathology in aged Grn$^{-/-}$ mice

To further explore the possible cause of sudden death in ageing Grn$^{-/-}$ mice, we monitored a cohort of animals from 15 months of age. Except for slightly reduced grooming in Grn$^{-/-}$ mice, no other features were discernible. Moreover, reduced grooming was not followed by immediate death, with many poorly groomed Grn$^{-/-}$ mice surviving for several months. In addition, we euthanized and examined 22-month-old Grn$^{-/-}$ mice along with their littermate controls. No gross hyper- or atrophic changes in visceral or thoracic organs were observed in Grn$^{-/-}$ mice on general autopsy. No obvious histopathological alterations, other than changes related to ageing, were observed in the heart, gastrointestinal tract, lungs, kidney, and spleen. However, we observed remarkable cytological alterations in the livers of old Grn$^{-/-}$ mice. Disarrayed masses of hepatic plates in liver parenchyma were present along with increased microvacuolation, lipofuscinosis, and hyalinosis (Figures 6A and 6B). Regenerative changes were also observed such as karyomegaly, cytomegaly, and polyploidy of hepatocytes (Figure 6A), along with abnormal bile duct proliferation (Figure 6B). Furthermore, the livers of 22-month-old Grn$^{-/-}$ mice also showed prominent aggregates of round-to-polygonal foamy histiocytes within sinusoids in the absence of acid fast bacilli or other inflammatory features (Figure 6C). In contrast, only cytological changes related to normal ageing were observed in Wt control mice (Figures 6D and 6E). Intense lysosomal staining of cathepsin D was also present in histiocytes and macrophages in Grn$^{-/-}$ mice (Figures 6F and 6G) compared with Wt mice (Figure 6H), suggesting lysosomal turnover defects due to Grn deficiency. Very rarely, we also observed infiltration in portal areas of lymphocytes, histiocytes, and neutrophils in the absence of significant cholestasis or fibrosis. Although we cannot exclude the possibility that such acute abscesses might progress to have fatal consequences, more importantly, the observed lysosomal turnover defects and increased lipofuscinosis in the liver and

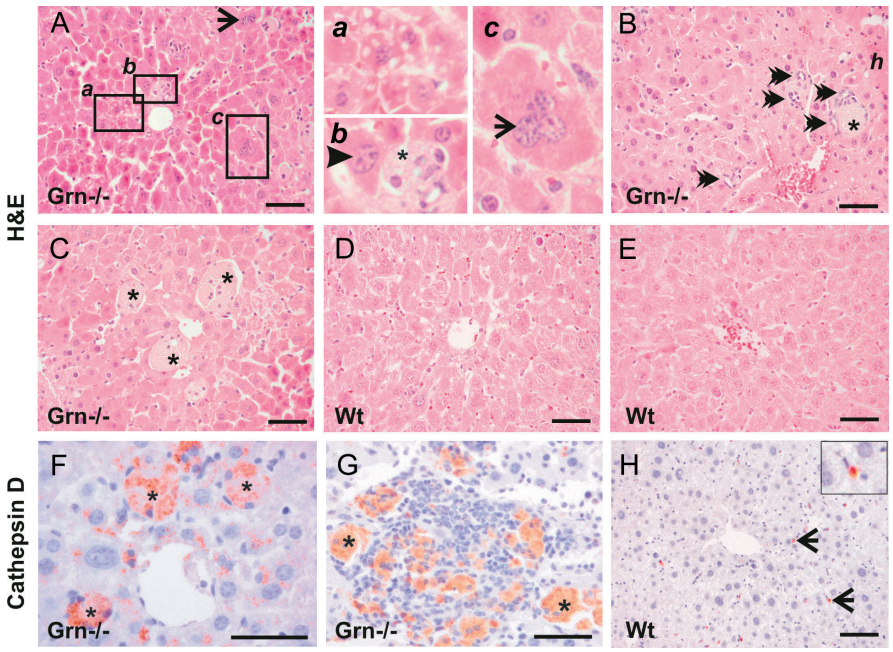

Figure 6. Hepatic cytological alterations in Grn$^{-/-}$ mice. (A) 22-month-old Grn$^{-/-}$ mice showing microvacuolation in the periportal region (inset a) accompanied by regenerative changes with karyomegaly (inset b, arrowhead) and multi-nucleation (arrows; inset c). (B) Hyaline changes (h) with breakdown of tissue architecture and abnormal bile duct proliferation (double-headed arrows) were also present in 22-month-old Grn$^{-/-}$ mice, with (C) foamy histiocytes in the perivenular regions (asterisks) but also in periportal areas (asterisks in b and B). (D, E) Wt 22-month-old littermates did not show these changes other than age-related karyomegaly, cytomegaly, polyploidy, and hyalinosis. (F, G) Cathepsin D staining in the foamy histiocytes (asterisks in F and G), but also in hepatocytes and perisinusoidal Kupffer cells (F). Rarely inflammatory cellular infiltrate was observed in the absence of significant cholestasis or fibrosis, as shown here in 22.5-month-old Grn$^{-/-}$ mice. (H) Cathepsin D staining in Wt littermates was largely limited to perisinusoidal Kupffer cells (arrows and inset). Scale bars = 5 μm.

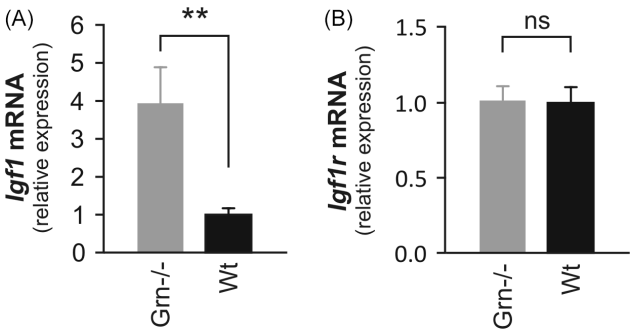

Figure 7. Increased *Igf1* mRNA levels in aged Grn$^{-/-}$ mice. qRT-PCR analysis on the brains of ≈ 18-month-old mice shows (A) a highly significant increase of Igf1 (3.95 ± 0.95; $p < 0.01$), while (B) Igf1R transcript levels remained unaltered (1.00 ± 0.105; $p > 0.05$) in Grn$^{-/-}$ compared with Wt mice. $N = 6$ animals per genotype and data are represented as mean ± SD.

brain suggest that Grn deficiency can lead to increased cellular ageing in mice.

While the precise reason for accelerated ageing in Grn$^{-/-}$ mice remains unknown, increased insulin-like growth factor (IGF)-1 signalling has been associated with decreased longevity and early onset of age-related disorders in diverse species [22]. Interestingly, we observed a highly significant 4-fold increase in *IGF-1* mRNA levels in the brains of aged Grn$^{-/-}$ mice compared with Wt controls, while the levels for IGFR1, the corresponding receptor, remained unchanged (Figures 7A and 7B; $p < 0.01$). Progranulin was identified as the only purified growth factor that could stimulate the growth of cultured cells lacking type 1 IGF receptor [23], suggesting parallels in IGFR and progranulin signalling. Therefore, disturbances of the IGF-1 axis could be an important mechanism responsible for the increased cellular ageing observed in our Grn$^{-/-}$ animals.

Discussion

Three constitutive Grn$^{-/-}$ mice have been established. Kayasuga *et al* established the first Grn$^{-/-}$ mice where *Grn* exons 2–13 were deleted [24]. Already at 3 months of age, these mice showed alterations in male-type behaviour including reduced frequency of ejaculation and elevated levels of aggression and anxiety [24]. Follow-up studies on these mice by two independent groups showed accelerated brain lipofuscinosis, ubiquitination, and gliosis beginning at 7 months of age [16,25]. These studies also showed increased mortality in Grn$^{-/-}$ mice but at different ages. While Ahmed *et al* reported increased embryonic and perinatal mortality [16], Ghoshal *et al* observed in the same mice increased adult-onset mortality but no embryonic or perinatal mortality [25]. Interestingly, no increased mortality was observed at any time-point for two independent Grn$^{-/-}$ knockout mouse models [26,27]. Yin

et al established germline $Grn^{-/-}$ mice in a C57Bl/6 background by excising the promoter and the first four exons of *Grn* [26]. Although these mice did not display impaired explorative behaviour, consistent with our behavioural data, deficits in spatial learning in the MWM task were observed in aged $Grn^{-/-}$ mice [25,28]. These studies also did not show any locomotor defects [25,28], although another study reported increased susceptibility to collagen-induced arthritis in $Grn^{-/-}$ mice [7]. This is consistent with the significantly decreased swimming speed noted in our $Grn^{-/-}$ mice, suggesting that subtle locomotive disorders could be a feature of $Grn^{-/-}$ mice. Furthermore, $Grn^{-/-}$ mice showed increased brain inflammation, but, interestingly, also increased phosphorylation of TDP-43 in the dentate gyrus and thalamus [26]. However, no increased TDP-43 phosphorylation was observed in another study using the same pTDP-43 antibody [16,25]. In a third $Grn^{-/-}$ mouse model, Petkau *et al* utilized a gene-trap vector to disrupt expression of *Grn*, instead expressing a lacZ/neomycin fusion protein under the control of the endogenous Grn promotor [27]. Moderate abnormalities in anxiety-related behaviours, social interactions, motor coordination, and novel object recognition were observed in 8-month-old $Grn^{-/-}$ mice. Additionally, altered synaptic connectivity and impaired synaptic plasticity were reported in 10- to 12-month-old $Grn^{-/-}$ mice [27].

While there could be several reasons for the discrepancies observed in the various $Grn^{-/-}$ mouse models, the mouse genetic background is a very strong driver of genetically engineered mouse phenotypes [29–31]. We showed that constitutive $Grn^{-/-}$ mice on a mixed 129/Sv and C57Bl/6 background are viable and are born in normal Mendelian frequencies, although increased mortality was observed beginning at 11 months of age. Compared with heterozygous $Grn^{+/-}$ mice, $Grn^{-/-}$ mice showed an $\approx$ 2-fold increased mortality at 11 months that increased exponentially to 5-, 7-, and 17-fold at 17, 20, and 23.5 months of age, respectively. Beginning at $\approx$ 6 months of age, $Grn^{-/-}$ mice also showed age-dependent activation of astrocytes and microglia, a common feature noted for all $Grn^{-/-}$ mouse models. This is interesting as Grn and its granulin peptides have been shown to be involved in inflammation, and Grn expression has also been shown to be up-regulated in microglia in many degenerative diseases and mouse models of degeneration [3,32]. These data suggest that overexpression of Grn by microglia is a consequence, rather than an upstream mechanism, in the microglial up-regulation observed in neurodegenerative diseases.

Another common feature shared between our $Grn^{-/-}$ mice and those previously reported [16,25,27] is an age-dependent increase in brain ubiquitination and accumulation of lipofuscin. Additionally, we report in our $Grn^{-/-}$ mice increased accumulation of the autophagy-related receptor p62 and increased expression of lysosomal proteases, including cathepsin D. These data suggest that dysfunction of both the ubiquitin–proteasome and the autophagy–lysosomal systems is involved in Grn deficiency-associated neurodegeneration, as also observed for FTLD-TDP patients [20].

Moreover, increased lipofuscinosis is also considered one of the most consistent and phylogenetically conserved cellular morphological changes associated with brain ageing [33]. Defects in the autophagy–lysosomal system are also associated with increased cellular ageing [34]. Thus, we postulate that constitutive Grn deficiency also leads to increased cellular ageing of non-neuronal tissue which in turn can cause increased mortality observed in ageing $Grn^{-/-}$ mice. Consistent with this premise, we have shown increased cellular ageing in several tissues, which was most remarkable in the liver, where we observed highly abnormal hepatic and ductal morphology and intensely stained cathepsin D-positive lysosomes within sinusoidal foamy histiocytes. Interestingly, while *GRN* mRNA levels have been shown to be moderate in the liver [35], a GRN homologue in zebrafish (GrnA) is suggested to play a role in liver growth regulation [36], and high levels of Grn protein and mRNA were found in areas of bile duct proliferation in a rodent cirrhotic liver model [37]. While the precise cause of increased cellular ageing in these tissues remains unknown, we have shown a 4-fold increase in IGF-1 levels without alterations in the cognate receptor, suggesting increased IGF signalling. Interestingly, IGF-1 signalling has been associated with decreased survival and lifespan in a variety of animal species, including higher vertebrates and mammals [22].

Lastly, consistent with other studies [16,38], we also showed that such ubiquitinated or lipofuscinous inclusions do not contain substantial amounts of TDP-43. Thus, awaiting more data, it appears that TDP-43 fragmentation and its ubiquitination could be a late event in FTLD pathogenesis. More interestingly, we also showed here that FL-TDP-43 is phosphorylated in aged $Grn^{-/-}$ mice brain and although no inclusions were observed, the FL-pTDP-43 is detergent-insoluble as it was consistently recovered from urea fractions. These data confirm our prior data on primary cortical neurons derived from these $Grn^{-/-}$ mice, where cellular stress associated with proteosomal blockage also led to increased insolubility of FL-phosphorylated TDP-43 [39]. We also showed that not only TDP-43, but also other protein substrates were phosphorylated at serine and threonine residues in $Grn^{-/-}$ mice, suggesting that loss of Grn might lead to perturbations of kinases or phosphatases, requiring further studies.

To conclude, we report a novel Grn FTLD mouse model where allelic loss of Grn does not cause fragmentation or aggregation of TDP-43 but does form ubiquitinated cellular inclusions and leads to increased phosphorylation states of many cellular proteins, including full-length nuclear TDP-43. We also report considerable abnormality of the autophagy–lysosomal system and increased cellular ageing of neuronal and non-neuronal tissue as a consequence of Grn

deficiency and a noteworthy up-regulation of IGF-1 which is known to reduce lifespan in a variety of animal species.

Acknowledgment

We thank Dr Manuela Neumann for the TDP-43 C-terminal antibody, Veerle Smits for support with experimental mouse work, and the personnel of the VIB Genetic Service Facility (http://www.vibgeneticservice facility.be) for genetic analyses. This work was supported in part by the Inter-university Attraction Poles Programme of the Belgian Science Policy Office, the Medical Foundation Queen Elisabeth (GSKE), the Foundation for Alzheimer Research (SAO/FRMA), the Methusalem Programme of the Flemish Government, the Research Foundation Flanders (FWO), the Agency for Innovation through Science and Technology Flanders (IWT), and the Special Research Fund of the University of Antwerp, Belgium. The research was performed in the frame of the international consortium of Centers of Excellence in Neurodegenerative Brain Diseases (CoEN; http://www.coen.org/) supported by the VIB (CVB) and DZNE (CH). JJ and SP received a PhD fellowship of the IWT, and GK of the FWO. DVD received a postdoctoral fellowship of the FWO.

Author contribution statement

SK-S designed the study. HW, GK, JJ, SP, and DVD conceived and carried out experiments and analysed data. SK-S and PPDD conceived experiments and analysed data. IC and GJ carried out experiments. CVB analysed and interpreted data. HW, GK, CVB, and SK-S wrote the manuscript. AC and CH generated and verified mouse Grn antibody.

References

Note: References 40–42 are cited in the Supporting information to this article.

1. Baker M, Mackenzie IR, Pickering-Brown SM, *et al*. Mutations in progranulin cause tau-negative frontotemporal dementia linked to chromosome 17. *Nature* 2006; **442**: 916–919.
2. Cruts M, Gijselinck I, van der Zee J, *et al*. Null mutations in progranulin cause ubiquitin-positive frontotemporal dementia linked to chromosome 17q21. *Nature* 2006; **442**: 920–924.
3. He Z, Bateman A. Progranulin (granulin-epithelin precursor, PC-cell-derived growth factor, acrogranin) mediates tissue repair and tumorigenesis. *J Mol Med* 2003; **81**: 600–612.
4. Van Damme P, Van Hoecke A, Lambrechts D, *et al*. Progranulin functions as a neurotrophic factor to regulate neurite outgrowth and enhance neuronal survival. *J Cell Biol* 2008; **181**: 37–41.
5. Kumar-Singh S. Progranulin and TDP-43: mechanistic links and future directions. *J Mol Neurosci* 2011; **45**: 561–573.
6. Hu F, Padukkavidana T, Vaegter CB, *et al*. Sortilin-mediated endocytosis determines levels of the frontotemporal dementia protein, progranulin. *Neuron* 2010; **68**: 654–667.
7. Tang W, Lu Y, Tian QY, *et al*. The growth factor progranulin binds to TNF receptors and is therapeutic against inflammatory arthritis in mice. *Science* 2011; **332**: 478–484.
8. Neumann M, Sampathu DM, Kwong LK, *et al*. Ubiquitinated TDP-43 in frontotemporal lobar degeneration and amyotrophic lateral sclerosis. *Science* 2006; **314**: 130–133.
9. Arai T, Hasegawa M, Akiyama H, *et al*. TDP-43 is a component of ubiquitin-positive tau-negative inclusions in frontotemporal lobar degeneration and amyotrophic lateral sclerosis. *Biochem Biophys Res Commun* 2006; **351**: 602–611.
10. Mackenzie IR, Neumann M, Bigio EH, *et al*. Nomenclature for neuropathologic subtypes of frontotemporal lobar degeneration: consensus recommendations. *Acta Neuropathol* 2009; **117**: 15–18.
11. Hasegawa M, Arai T, Nonaka T, *et al*. Phosphorylated TDP-43 in frontotemporal lobar degeneration and amyotrophic lateral sclerosis. *Ann Neurol* 2008; **64**: 60–70.
12. Wils H, Kleinberger G, Janssens J, *et al*. TDP-43 transgenic mice develop spastic paralysis and neuronal inclusions characteristic of ALS and frontotemporal lobar degeneration. *Proc Natl Acad Sci U S A* 2010; **107**: 3858–3863.
13. Igaz LM, Kwong LK, Xu Y, *et al*. Enrichment of C-terminal fragments in TAR DNA-binding protein-43 cytoplasmic inclusions in brain but not in spinal cord of frontotemporal lobar degeneration and amyotrophic lateral sclerosis. *Am J Pathol* 2008; **173**: 182–194.
14. Sampathu DM, Neumann M, Kwong LK, *et al*. Pathological heterogeneity of frontotemporal lobar degeneration with ubiquitin-positive inclusions delineated by ubiquitin immunohistochemistry and novel monoclonal antibodies. *Am J Pathol* 2006; **169**: 1343–1352.
15. Kumar-Singh S, Pirici D, McGowan E, *et al*. Dense core plaques in Tg2576 and PSAPP mouse models of Alzheimer's disease are centered on vessel walls. *Am J Pathol* 2005; **167**: 527–543.
16. Ahmed Z, Sheng H, Xu YF, *et al*. Accelerated lipofuscinosis and ubiquitination in granulin knockout mice suggests a role for progranulin in successful aging. *Am J Pathol* 2010; **177**: 311–324.
17. Lehman NL. The ubiquitin proteasome system in neuropathology. *Acta Neuropathol* 2009; **118**: 329–347.
18. Riga D, Riga S, Halalau F, *et al*. Brain lipopigment accumulation in normal and pathological aging. *Ann N Y Acad Sci* 2006; **1067**: 158–163.
19. Komatsu M, Waguri S, Koike M, *et al*. Homeostatic levels of p62 control cytoplasmic inclusion body formation in autophagy-deficient mice. *Cell* 2007; **131**: 1149–1163.
20. Ju JS, Weihl CC. Inclusion body myopathy, Paget's disease of the bone and fronto-temporal dementia: a disorder of autophagy. *Hum Mol Genet* 2010; **19**: R38–R45.
21. Igaz LM, Kwong LK, Chen-Plotkin A, *et al*. Expression of TDP-43 C-terminal fragments *in vitro* recapitulates pathological features of TDP-43 proteinopathies. *J Biol Chem* 2009; **284**: 8516–8524.
22. Rincon M, Rudin E, Barzilai N. The insulin/IGF-1 signaling in mammals and its relevance to human longevity. *Exp Gerontol* 2005; **40**: 873–877.
23. Xu SQ, Tang D, Chamberlain S, *et al*. The granulin/epithelin precursor abrogates the requirement for the insulin-like growth factor 1 receptor for growth *in vitro*. *J Biol Chem* 1998; **273**: 20078–20083.
24. Kayasuga Y, Chiba S, Suzuki M, *et al*. Alteration of behavioural phenotype in mice by targeted disruption of the progranulin gene. *Behav Brain Res* 2007; **185**: 110–118.
25. Ghoshal N, Dearborn JT, Wozniak DF, *et al*. Core features of frontotemporal dementia recapitulated in progranulin knockout mice. *Neurobiol Dis* 2012; **45**: 395–408.
26. Yin F, Banerjee R, Thomas B, *et al*. Exaggerated inflammation, impaired host defense, and neuropathology in progranulin-deficient mice. *J Exp Med* 2009; **207**: 117–128.

27. Petkau TL, Neal SJ, Milnerwood A, *et al*. Synaptic dysfunction in progranulin-deficient mice. *Neurobiol Dis* 2012; **45**: 711–722.
28. Yin F, Dumont M, Banerjee R, *et al*. Behavioral deficits and progressive neuropathology in progranulin-deficient mice: a mouse model of frontotemporal dementia. *FASEB J* 2010; **24**: 4639–4647.
29. Doetschman T. Interpretation of phenotype in genetically engineered mice. *Lab Anim Sci* 1999; **49**: 137–143.
30. Yang JT, Bader BL, Kreidberg JA, *et al*. Overlapping and independent functions of fibronectin receptor integrins in early mesodermal development. *Dev Biol* 1999; **215**: 264–277.
31. Tominaga K, Matsuda J, Kido M, *et al*. Genetic background markedly influences vulnerability of the hippocampal neuronal organization in the 'twitcher' mouse model of globoid cell leukodystrophy. *J Neurosci Res* 2004; **77**: 507–516.
32. Pereson S, Wils H, Kleinberger G, *et al*. Progranulin expression correlates with dense-core amyloid plaque burden in Alzheimer disease mouse models. *J Pathol* 2009; **219**: 173–181.
33. Porta EA. Pigments in aging: an overview. *Ann N Y Acad Sci* 2002; **959**: 57–65.
34. Rubinsztein DC, Marino G, Kroemer G. Autophagy and aging. *Cell* 2011; **146**: 682–695.
35. Daniel R, He Z, Carmichael KP, *et al*. Cellular localization of gene expression for progranulin. *J Histochem Cytochem* 2000; **48**: 999–1009.
36. Li YH, Chen MH, Gong HY, *et al*. Progranulin A-mediated MET signaling is essential for liver morphogenesis in zebrafish. *J Biol Chem* 2010; **285**: 41001–41009.
37. Guerra RR, Trotta MR, Parra OM, *et al*. Modulation of extracellular matrix by nutritional hepatotrophic factors in thioacetamide-induced liver cirrhosis in the rat. *Braz J Med Biol Res* 2009; **42**: 1027–1034.
38. Dormann D, Capell A, Carlson AM, *et al*. Proteolytic processing of TAR DNA binding protein-43 by caspases produces C-terminal fragments with disease defining properties independent of progranulin. *J Neurochem* 2009; **110**: 1082–1094.
39. Kleinberger G, Wils H, Joris G, *et al*. Increased caspase activation and decreased TDP-43 solubility in progranulin knockout cortical cultures. *J Neurochem* 2010; **115**: 735–747.
40. Spandidos A, Wang X, Wang H, *et al*. PrimerBank: a resource of human and mouse PCR primer pairs for gene expression detection and quantification. *Nucleic Acids Res* 2010; **38**: D792–D799.
41. Pirici D, van der Zee J, Vandenberghe R, *et al*. Characterization of ubiquitinated intraneuronal inclusions in a novel Belgian frontotemporal lobar degeneration family. *J Neuropathol Exp Neurol* 2006; **65**: 289–301.
42. Paxinos G, Franklin KBJ. *The Mouse Brain in Stereotaxic Coordinates*. Academic Press: London, 2001.

SUPPORTING INFORMATION ON THE INTERNET

The following supporting information may be found in the online version of this article.

Supplementary methods

Figure S1. Mouse Grn immunoblot showed reduced FL progranulin levels in brain lysates of $Grn^{+/-}$ mice and was absent in $Grn^{-/-}$ mice.

Figure S2. Subtle cognitive alterations in aged $Grn^{-/-}$ mice.

Figure S3. Increased gliosis in aged $Grn^{-/-}$ mice.

Figure S4. Increased accumulation of ubiquitin, lipofuscin, and p62 in various brain areas of $Grn^{-/-}$ mice.

Figure S5. No pathological alterations in (A, B) pTau, (C) α-synuclein, and (D) Fus by immunohistochemical analysis.

Figure S6. Increased phosphorylation of full-length (FL) TDP-43 in aged $Grn^{-/-}$ mice confirmed with polyclonal anti-phospho 403/404 TDP-43 (pTDP 403/404) antibody.

Figure S7. (A) Cleaved caspase-3 immunohistochemistry showing occasional caspase-3 staining in the cortex of $Grn^{-/-}$ but also of Wt mice. (B) TUNEL staining showed no obvious increase in apoptotic neurons in $Grn^{-/-}$ mice compared with Wt mice. (C) Immunoblotting with anti-caspase-3 or anti-PARP antibodies could also not detect any differences in apoptosis between $Grn^{-/-}$ and Wt mice.

Figure S8. (A) Full-length (FL) pTDP-43 was predominantly recovered from sarkosyl-soluble and -insoluble (urea) fractions in a sequential extraction of $Grn^{-/-}$ mouse brain lysates (lanes 1–4) and in the urea fractions of $Grn^{-/-}$ brain from the RIPA/urea protein extraction protocol (lanes 5 and 6). (B) FL pTDP-43 was predominantly recovered from the nuclear fraction and was absent in the cytoplasmic fraction.

Table S1. Antibodies used in the characterization of $Grn^{-/-}$ mice.

Table S2. qRT-PCR primers used in the characterization of $Grn^{-/-}$ mice.